Measurement of the Tensor Observable A_{zz} using SoLID

A Letter of Intent to Jefferson Lab PAC 49

E. Long, [†] [‡] K. Slifer,[†]

L. Kurbany, M. McClellan, E. Mustafa, D. Ruth

University of New Hampshire, Durham, NH 03861

We propose to measurement of the tensor asymmetry A_{zz} in the quasi-elastic through DIS region through the tensor polarized D(e, e')X channel in the SoLID detector; an asymmetry that is sensitive to the nucleon-nucleon potential. Previous measurements of A_{zz} have been used to extract b_1 in the DIS region and T_{20} in the elastic region. In the quasi-elastic region, A_{zz} data will be used to compare light cone calculations with variation nucleon-nucleon calculations, and is an important quantity to determine for understanding tensor effects, such as the dominance of pn correlations in nuclei.

In the quasi-elastic region, A_{zz} was first calculated in 1988 by Frankfurt and Strikman, using the Hamada-Johnstone and Reid soft-core wave functions [1]. Calculations by M. Sargsian revisit A_{zz} in the $x > 1$ range using virtual-nucleon and light-cone methods, which differ by up to a factor of two [2].

We propose an experimental determination of A_{zz} utilizing the same equipment as the co-submitted b_1 Letter of Intent that would also use the SoLID detector in Hall A. A_{zz} will be measured over the course of 14 days equally split between two beam energies of 6.6 GeV and 8.8 GeV, with 4.9 additional days of overhead. This measurement would be taken simultaneously with the co-submitted b_1 Letter of Intent.

[‡] Spokesperson

[§] Contact: elena.long@unh.edu

Contents

1. Background

The deuteron is the simplest composite nuclear system, and in many ways it is as important to understanding bound states in QCD as the hydrogen atom was to understanding bound systems in QED. Our experimental and theoretical understanding of the deuteron remains unsatisfying.

Due to their small size and simple structure, tensor polarized deuterons are ideal for studying nucleon-nucleon interactions. Tensor polarization enhances the D-state contribution, which compresses the deuteron [3], making the system more sensitive to short-range QCD effects. Understanding the nucleon-nucleon potential of the deuteron is essential for understanding short-range correlations as they are largely dependent on the tensor force [4]. We can resolve the short-range structure of nuclei on the level of nucleon and hadronic constituents by utilizing processes that transfer to the nucleon constituents both energy and momentum larger than the scale of the NN short-range correlations, particularly at $Q^2 > 1\ (\mathrm{GeV}/c)^2$.

By taking a ratio of cross sections from electron scattering from tensor-polarized and unpolarized deuterons, the S and D-wave states can be disentangled, leading to a fuller understanding of the repulsive nucleon core. A measurement of A_{zz} is sensitive to the $\frac{D^2-SD}{S^2+D^2}$ ratio and it's evolution with increasing minimal momentum of the struck nucleon. Originally calculated by L. Frankfurt and M. Strikman [1], this has recently been revisited by M. Sargsian, who calculated A_{zz} in this region using a light cone approach and a virtual nucleon approach. The calculations vary by up to a factor of 2.

In the deep inelastic region, A_{zz} will simultaneously be measured to extract the tensor structure function b_1 by the relation $A_{zz} \propto \frac{b_1}{F_1^D}$.

1.1. Probing the Deuteron Wavefunction

It was suggested for some time [5] that to resolve the microscopic structure of nuclei one needs to study scattering at sufficiently large momentum transfer and large relative momenta of the

produced nucleons. This logic was confirmed [4] by a series of experiments at SLAC [6] and JLab [7, 8] that directly observed short-range correlations (SRC) in a series of nuclei, and established a similar effect of SRC in the deuteron and in heavier nuclei with pn correlations giving the dominant contribution. Hence, the deuteron serves as a "hydrogen atom" for the studies of the microscopic short-range structure of the nuclei since it is the simplest nuclei that follows SRC scaling.

To achieve further progress, it is necessary to improve our knowledge of the deuteron wave function at high momenta, and to separate the S and D contributions to the high momentum component of the deuteron. The dominance of the D-wave at a large range of the nucleon momenta is expected in a range of the theoretical models, as demonstrated in Fig. 1, but experimentally it was probed in a rather indirect way via measurement of T_{20} for the deuteron form factor [9]. Still, the knowledge of S/D ratio for large momenta is rather poor. Indeed, all wavefunctions are constrained by low energy data to reproduce the S/D ratio at small momenta while the overall probability of the D-wave in the deuteron differs by a factor up to 1.5, leading to a large difference of the S/D ratio at large momenta.

The S and D-states are related to the tensor asymmetry A_{zz} by [1]

$$A_{zz} \propto \frac{\frac{1}{2}w^2(k) - u(k)w(k)\sqrt{2}}{u^2(k) + w^2(k)}, \tag{1}$$

where $u(k)$ is the S-state wave function and $w(k)$ is the D-state wave function. Additionally, measuring A_{zz} at lower Q^2 will map out the transition from hadronic to partonic degrees of freedom.

Ratios of inclusive cross sections at $x > 1$ has demonstrated an early onset of the scaling of the ratios when plotted as a function of the light-cone fraction of the struck nucleon momentum. As a result, the ratios provide a direct measurement of the ratio of the high momentum components in nuclei. Similarly, one can expect that in the case of scattering from the polarized deuteron we expect the early scaling for the asymmetry when plotted as a function of the minimal struck nucleon momentum or the light cone fraction in the A(e, e') case. It was observed at JLab that the scaling of the ratios set in starting at $Q^2 \sim 1$ GeV^2 [7] so covering the range of Q^2 up to 2 GeV^2 will be sufficient to measure the S/D ratios in an interesting momentum range.

It is worth noting here that in addition to comparing predictions for the different wave functions, one expects to be able to distinguish between non-relativistic and light cone quantum mechanic

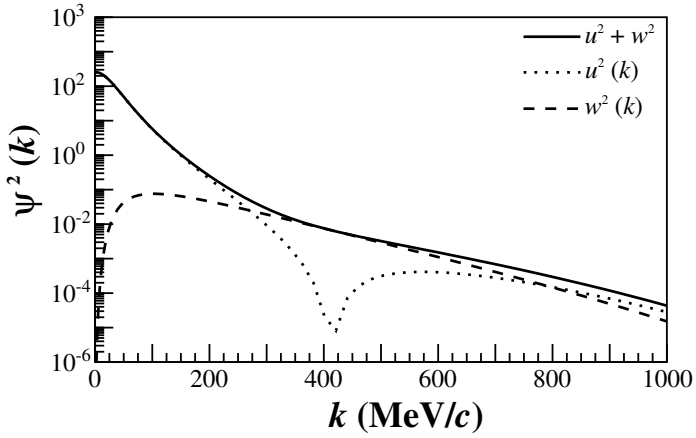

FIG. 1. The AV18 [10] deuteron wave-function, showing the dominance of the D-state (dashed) in comparison to the S-state (dotted) in the full wavefunction (solid) at high momentum ($k > 300$ Mev/c).

models. The principal difference between the models is the relation between the spectator momentum and momentum in the wave function. In the nonrelativistic model they coincide, while in the light cone model the relation is non-linear starting at $k \sim 250\,\mathrm{MeV}/c$. This difference is most clearly manifested in the scattering from the polarized deuteron due to a strong dependence of the S/D ratio on the nucleon momentum.

1.2. Study of the Relativistic NN Bound System

One of the important issues in studying of nuclear structure at short distances is the relativistic description of the bound system. This is an important issue also in understanding the QCD medium effect with recent studies indicating that parton distribution modifications in nuclei are proportional to the high momentum component of nuclear wave function.

The deuteron is the simplest bound system and naturally any self-consistent attempt to understand the relativistic effects in the bound nuclear systems should start with the deuteron. The issue of the relativistic description of the deuteron has long history with extensive research that started in late 1970's [5, 11–13].

The experimental studies of the relativistic effects in the deuteron up to now include the large Q^2 elastic ed scattering [14], however due to complexities in the reaction mechanism [15] the relativistic effects were difficult to isolate.

The inclusive D(e,e')X experiments from tensor-polarized deuterons at $Q^2 > 1$ GeV^2 and $x > 1$ region gives a new possibility to probe the relativistic structure of the deuteron. In this case the use of the tensor polarized deuteron allows us to prepare the nucleus in the most compact state in which, due to the absence of the pure S-wave^2 contribution, the system in average is sensitive to the higher moment of the nucleon in the deuteron. At large $Q^2 > 1$ GeV^2 kinematics, the probed longitudinal momenta of the bound nucleon $p_z \approx m_N(1-x)$, or the light cone momentum fraction $\alpha \geq x$. Because of these kinematic conditions and the absence of the large S-wave^2 contribution, one expects a measurable relativistic effects already at $x \leq 1.2$.

The biggest advantage is that one expects less uncertainty due to the choice of the NN potential and reaction dynamics due to relatively small values of the bound nucleon momenta involved (≥ 200 MeV$/c$).

The sensitivity to relativistic effects is estimated using the theoretical calculations based on two very different approaches. The first approach treats the virtuality of the bound nucleon within a description of the deuteron in the lab. frame with treating the interacting nucleon as being virtual (virtual nucleon, or VN, approximation) by taking the residue over the energy of the spectator nucleon. In this case, the deuteron wave function satisfies the covariant equation of two-nucleon bound system with spectator being on energy shell [16, 17].

Another approach is based on the observation that high energy processes evolve along the light-cone (LC). Therefore, it is natural to describe the reaction within the light-cone non-covariant framework [5]. Negative energy states do not enter in this case, though one has to take into account so called instantaneous interactions. In the approximation when non-nucleonic degrees of freedom in the deuteron wave function can be neglected, one can unambiguously relate the light-cone wave functions to those calculated in the lab. frame by introducing the LC pn relative three momentum,

$$k = \sqrt{\frac{m^2 + p_t^2}{\alpha(2-\alpha)} - m^2}. \tag{2}$$

2. The Proposed Experiment

We propose to measure the tensor asymmetry A_{zz} from inclusive electron scattering from polarized deuterons in the region of $0.1 < x < 2.0$ utilizing the SoLID detector in Hall A.

Fig. 2 show the planned kinematic coverage utilizing the SOLID forward and large angle detectors with beam energies of $6.6\ \mathrm{GeV}$ and $8.8\ \mathrm{GeV}$. This data can be taken simultaneously with a DIS measurement of b_1, which is being submitted as a separate Letter of Intent.

The polarized ND_3 target is discussed in section 2.3. The magnetic field of the target will be held constant along the beamline at all times, while the target state is alternated between a polarized and unpolarized state. The tensor polarization and packing fraction used in the rates estimate are 25% and 0.65, respectively. The dilution fraction in the range of this measurement is shown in Fig. 3. With an incident electron beam current of 100 nA, the expected deuteron luminosity is 1.36×10^{35} / cm^2·s^1.

The SoLID detector was incorporated assuming a momentum resolution of $dP/P = 2\%$, $d\theta = 0.6\ \mathrm{mrad}$, and $d\phi = 5\ \mathrm{mrad}$. The forward detector assumes an acceptance of $8^\circ \leq \theta \leq 14.8^\circ$ and $1.0\ \mathrm{GeV}/c \leq P \leq 7.0\ \mathrm{GeV}/c$. The large angle detector assumes an acceptance of $16^\circ \leq \theta \leq 24^\circ$ and $3.5\ \mathrm{GeV}/c \leq P \leq 7.0\ \mathrm{GeV}/c$.

Projected uncertainties in A_{zz} are summarized in Table II and displayed in Fig. 4.

A total of 14 days of beam time is requested for production data, with an additional 4.9 days of expected overhead.

2.1. Experimental Method

The measured double differential cross section for a spin-1 target is characterized by a vector polarization P_z and tensor polarization P_{zz} is expressed as,

$$\frac{d^2\sigma_p}{d\Omega dE'} = \frac{d^2\sigma_u}{d\Omega dE'}\left(1 - P_z P_B A_1 + \frac{1}{2} P_{zz} A_{zz}\right), \tag{3}$$

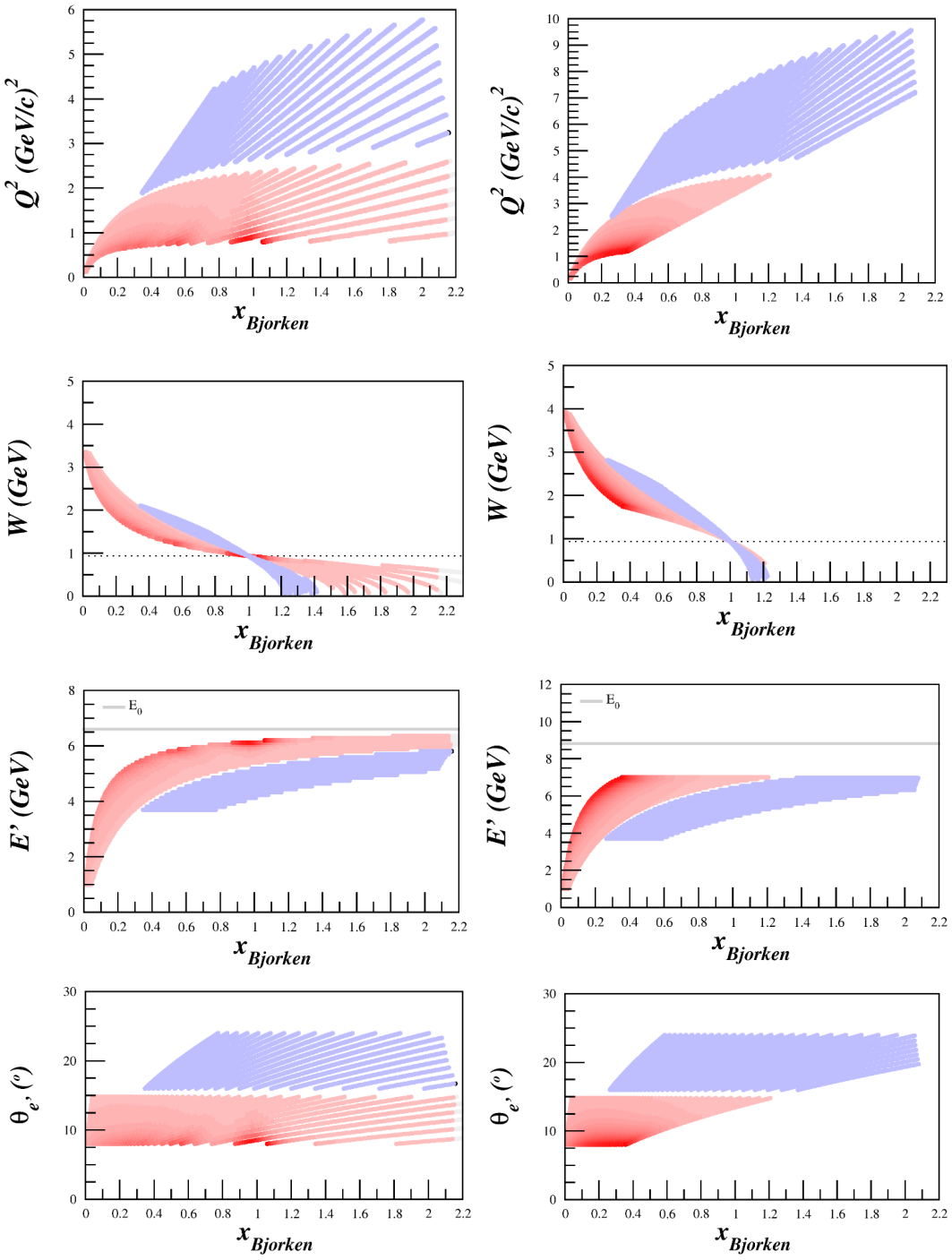

FIG. 2. Kinematic coverage for the proposed measurement. Left plots are at $E = 6.6$ GeV and right plots are at $E = 8.8$ GeV.

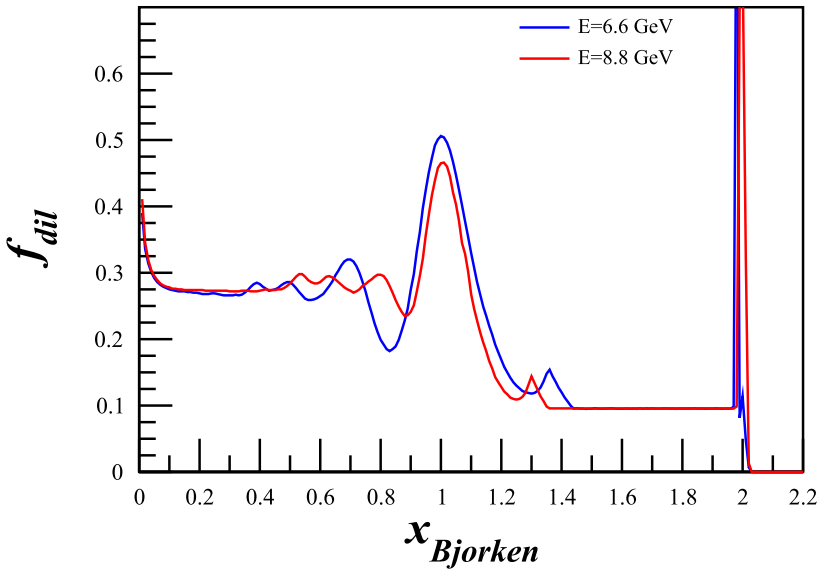

FIG. 3. Projected dilution factor covering the entire x range to be measured using a combination of P. Bosted's [18] and M. Sargsian's [19] code.

where, σ_p (σ_u) is the polarized (unpolarized) cross section, P_B is the incident electron beam polarization, and A_1 (A_{zz}) is the vector (tensor) asymmetry of the virtual-photon deuteron cross section. This allows us to write the polarized tensor asymmetry with positive tensor polarization using an unpolarized electron beam as

$$A_{zz} = \frac{2}{P_{zz}} \left(\frac{\sigma_p - \sigma_u}{\sigma_u} \right). \tag{4}$$

The tensor polarization is given by

$$P_{zz} = \frac{n_+ - 2n_0 + n_-}{n_+ + n_- + n_0}, \tag{5}$$

where n_m represents the population in the $m_z = +1, -1$, or 0 state.

Eq. 4 reveals that the asymmetry A_{zz} compares two different cross sections measured under different polarization conditions of the target: positively tensor polarized and unpolarized. To obtain the relative cross section measurement in the same configuration, the same target cup and material will be used at alternating polarization states (polarized vs. unpolarized), and the magnetic field providing the quantization axis will be oriented along the beamline at all times. This field will always be held at the same value, regardless of the target material polarization state. This process

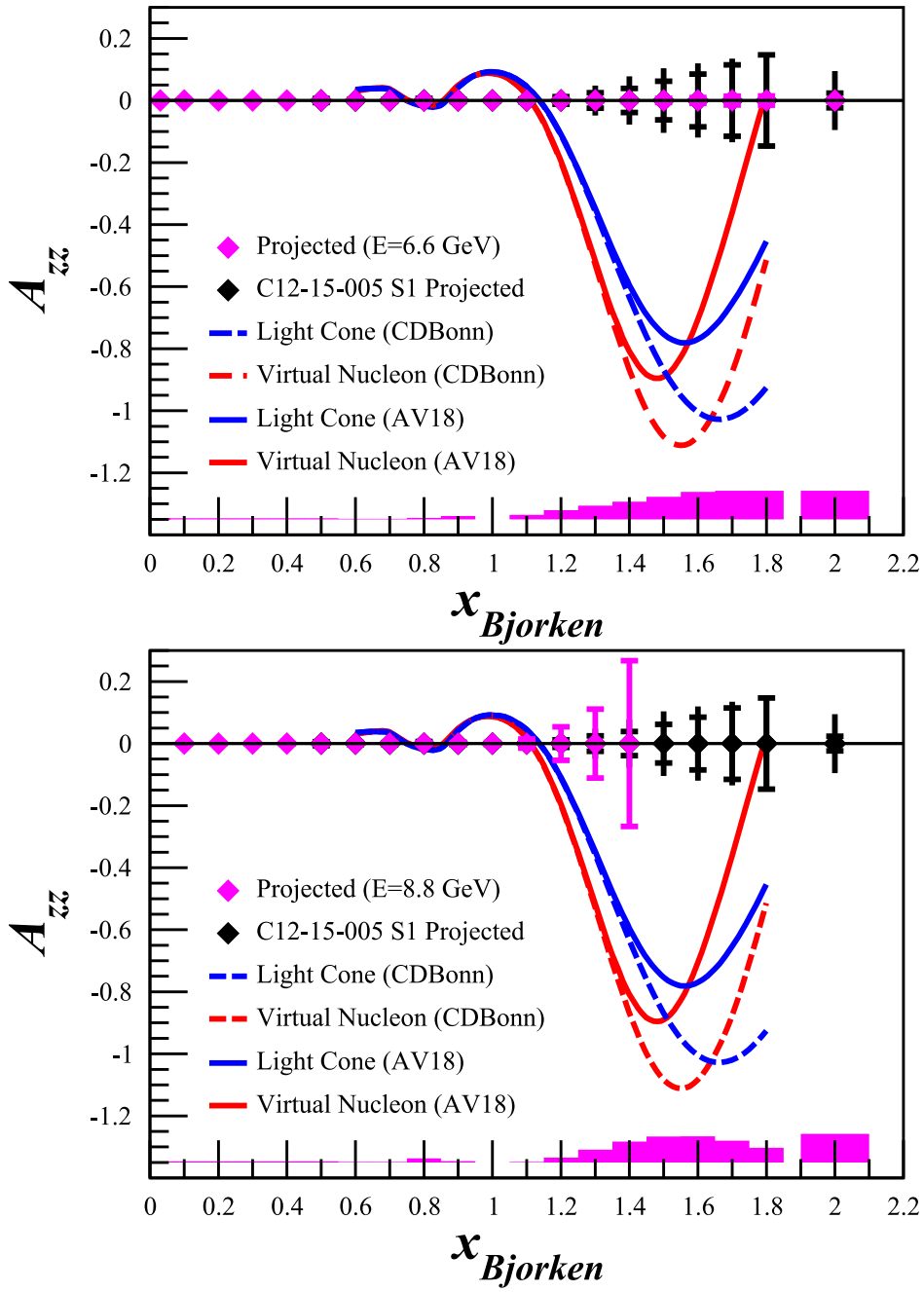

FIG. 4. Projected statistical errors for the tensor asymmetry A_{zz} with 14 days of beam time at beam energies of 6.6 GeV (top) and 8.8 GeV (bottom). The band represents the systematic uncertainty. Black bars indicate proposed uncertainties of the C12-15-005 experiment. Also shown are $Q^2 = 1.5$ $(\mathrm{GeV}/c)^2$ calculations provided by M. Sargsian for using a light cone and virtual nucleon model using both the AV18 and CD-Bonn potentials.

ensures that the acceptance remains consistent within the stability (10^{-4}) of the super conducting magnet.

Since many of the factors involved in the cross sections cancel in the ratio, Eq. 4 can be expressed in terms of the charge normalized, efficiency corrected numbers of tensor polarized (N_p) and unpolarized (N_u) counts,

$$A_{zz} = \frac{2}{f P_{zz}} \left(\frac{N_p - N_u}{N_u} \right). \tag{6}$$

The dilution factor f corrects for the presence of unpolarized nuclei in the target and is defined by

$$f = \frac{N_D \sigma_D}{N_N \sigma_N + N_D \sigma_D + \sum_A N_A \sigma_A}, \tag{7}$$

where N_D is the number of deuterium nuclei in the target and σ_D is the corresponding inclusive double differential scattering cross section, N_N is the nitrogen number of scattered nuclei with cross section σ_N, and N_A is the number of other scattering nuclei of mass number A with cross section σ_A. As has been noted in previous work [1], the dilution factor at high x drops off considerably until the SRC plateau region, as shown in Fig. 3. By using a high-luminosity solid target and a low scattering angle $\theta_{e'}$, this effect will be counteracted.

The dilution factor can be written in terms of the relative volume ratio of ND_3 to LHe in the target cell, otherwise known as the packing fraction p_f. In our case of a cylindrical target cell oriented along the magnetic field,the packing fraction is exactly equivalent to the percentage of the cell length filled with ND_3.

If the time is evenly split between scattering off of polarized and unpolarized ND_3, the time necessary to achieve the desired precision δA is:

$$T = \frac{N_p}{R_p} + \frac{N_u}{R_u} = \frac{8}{f^2 P_{zz}^2} \left(\frac{R_p (R_u + R_p)}{R_u^3} \right) \frac{1}{\delta A_{zz}^2} \tag{8}$$

where $R_{p(u)}$ is the polarized (unpolarized) rate and $N_{p(u)}$ is the total estimated number of polarized (unpolarized) counts to achieve the uncertainty δA_{zz}.

E (GeV)	Forward Det. Physics Rates (kHz)	Forward Det. Total Rates (kHz)	Large θ Det. Physics Rates (kHz)	Large θ Det. Total Rates (kHz)	Time (days)
6.6	151	540	1.25	4.4	7
8.8	67.1	239	1.01	3.56	7

TABLE I. Summary of the kinematics and physics rates using the SoLID detector.

$\overline{x}$	δA_{zz}^{stat} $\times 10^{-2}$	δA_{zz}^{sys} $\times 10^{-2}$
0.03	0.0135	0.362
0.1	0.0103	0.363
0.2	0.0132	0.354
0.3	0.0165	0.357
0.4	0.0204	0.357
0.5	0.027	0.361
0.6	0.0275	0.150
0.7	0.0375	0.155
0.8	0.079	0.484
0.9	0.0384	1.100
1	0.026	0.002
1.1	0.0422	1.45
1.2	0.139	2.94
1.3	0.294	4.42
1.4	0.341	5.69
1.5	0.667	7.29
1.6	0.931	8.83
1.7	1.43	9.20
1.8	1.49	9.20
2	0.212	9.20

TABLE II. Summary of the expected statistical uncertainty after combining overlapping x-bins for $E = 6.6$ GeV.

$\overline{x}$	δA_{zz}^{stat} $\times 10^{-2}$	δA_{zz}^{sys} $\times 10^{-2}$
0.1	0.0142	0.333
0.2	0.0177	0.334
0.3	0.0223	0.321
0.4	0.03	0.319
0.5	0.0457	0.318
0.6	0.0707	0.152
0.7	0.113	0.158
0.8	0.209	1.34
0.9	0.37	0.380
1	0.4	0.002
1.1	1.47	0.135
1.2	5.41	1.55
1.3	11.1	4.13
1.4	26.7	6.72

TABLE III. Summary of the expected statistical uncertainty after combining overlapping x-bins for $E = 8.8$ GeV.

2.2. Uncertainty Estimates

We discuss here the expected experimental and systematic uncertainties that we expect to contribute to the measurement.

2.2.1. Statistical Uncertainty

To investigate the statistical uncertainty we start with the equation for A_{zz} using measured counts for polarized data (N_p) and unpolarized data (N_u),

$$A_{zz} = \frac{2}{fP_{zz}} \left(\frac{N_p}{N_u} - 1 \right). \tag{9}$$

The statistical error with respect to counts is then

$$\delta A_{zz} = \frac{2}{fP_{zz}} \sqrt{\left(\frac{\delta N_p}{N_u} \right)^2 + \left(\frac{N_p \delta N_u}{N_u^2} \right)^2}. \tag{10}$$

For $\delta N_{p(u)} = \sqrt{N_{p(u)}}$, the uncertainty becomes

$$\delta A_{zz} = \frac{2}{fP_{zz}} \sqrt{\frac{N_p(N_u + N_p)}{N_u^3}}, \tag{11}$$

which can't be simplified further due to the large expected asymmetry.

The number of counts was calculated using a combination of P. Bosted's [18] and M. Sargsian's [19] code. The Bosted code was used for the lower $x < 1.1$ region, where effects of SRC scaling are expected to be negligible and to accurately determine the quasi-elastic peak. The Sargsian code was used for the $x > 1.1$ region due to its inclusion of SRC scaling effects.

2.2.2. Systematic Uncertainty

Table IV shows a list of the scale dependent uncertainties contributing to the systematic error in A_{zz}. With careful uncertainty minimization in polarization the relative error in vector polarization,

Source	Systematic
P_{zz} Polarimetry	12%
Dilution Factor	6.0%
Packing Fraction	3.0%
Trigger/Tracking Efficiency	1.0%
Acceptance	0.5%
Charge Determination	1.0%
Detector Resolution and Efficiency	1.0%
Total	14%

TABLE IV. Estimates of the scale dependent contributions to the systematic error of A_{zz}.

P_z, can be less than or equal to 3.9%, as was demonstrated for the proton in the recent E08-027/E08-007 experiment [20] and nearly as good for the deuteron using multiple techniques to measure the NMR signal as discussed in [21]. With the use of a positive tensor enhanced target it has been projected to be able to achieve a relative error in P_{zz} better than 12% [21]. The uncertainty from the dilution in the polarized target is estimated to be about 6% over the range of kinematics points of interest. We consider separately the uncertainty in the packing fraction of the ammonia target contributes at a level of less than 3%. Charge calibration and detector efficiencies are expected to be known better to 1%. Time dependent systematic effects were considered the same as in the C12-15-005 proposal.

2.3. Polarized Target

This experiment will use the JLab/UVa dynamically polarized solid ND_3 target operated in longitudinal mode. The target is typically operated with a specialized slow raster and beamline instrumentation capable of characterizing the low current 50-100 nA beam. All of these requirements have been met previously in Hall A. The polarized target (see Fig. 5), has been successfully used in

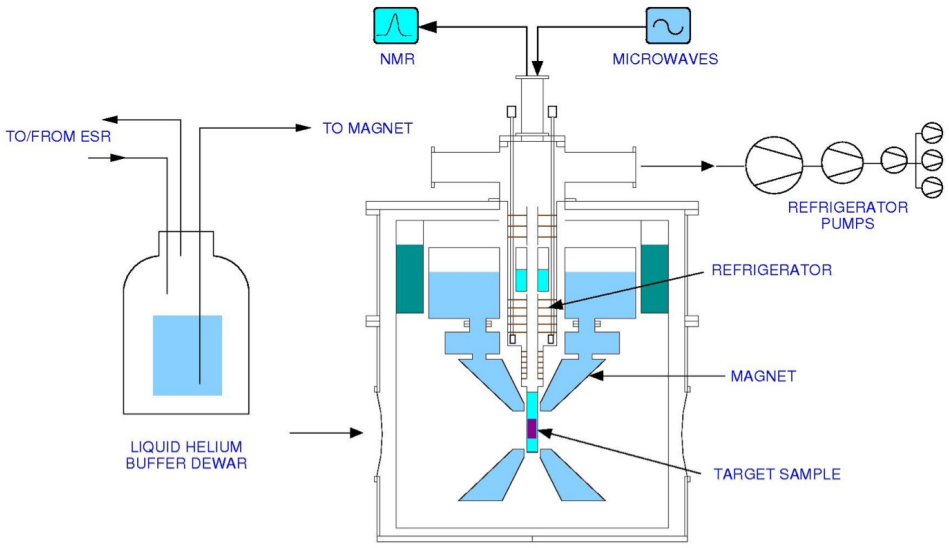

FIG. 5. Cross section view of the JLab/UVa polarized target. The proposed experiment will use the modified Hall B magnet, where the backwards-scattering cone is blocked with quench protection circuitry. Figure courtesy of C. Keith.

experiments E143, E155, and E155x at SLAC, and E93-026, E01-006 and E07-003, E08-027 and E08-007 at JLab. A similar target was used in Hall B for the EG1, EG4, and DVCS experiments.

The JLab/UVa target underwent significant renovation and improvement [22] during the recent g2p run. The magnet was replaced early in the run, and the target then performed consistently. A new 1 K refrigerator and target insert were designed and constructed by the JLab target group. The cryogenic pumping system has been overhauled. In particular, the older Alcatel 2060H rotary vane pumps have been replaced with new Pfeiffer DU065 magnetically coupled rotary vane pumps, and the pump controls are being refurbished. The target motion system has been rebuilt from scratch.

The target operates on the principle of Dynamic Nuclear Polarization, to enhance the low temperature (1 K), high magnetic field (5 T) polarization of solid materials by microwave pumping. The polarized target assembly contains several target cells of 3.0 cm length that can be selected individually by remote control to be located in the uniform field region of a superconducting Helmholtz pair. The permeable target cells are immersed in a vessel filled with liquid Helium and maintained at 1 K by use of a high power evaporation refrigerator. The coils have a 50°

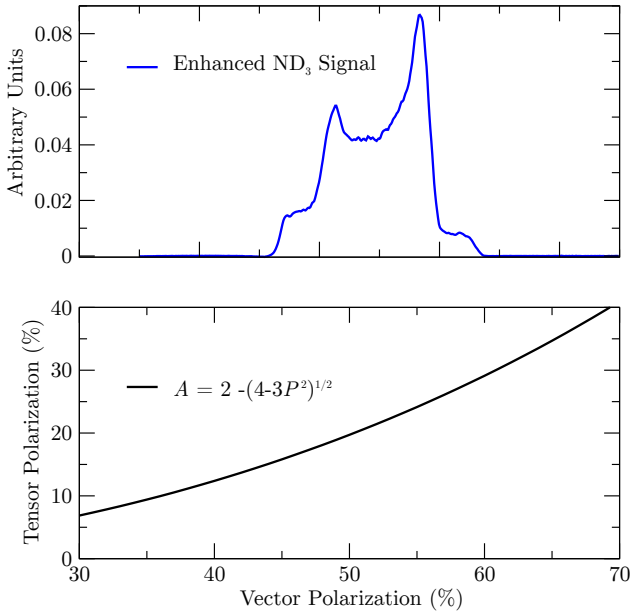

FIG. 6. **Top**: NMR signal for ND_3 with a vector polarization of approximately 50% from the GEN experiment. **Bottom**: Relationship between vector and tensor polarization in equilibrium, and neglecting the small quadrupole interaction.

conical shaped aperture along the beam axis which allow for unobstructed forward scattering.

The target material is exposed to microwaves to drive the hyperfine transition which aligns the nucleon spins. The heating of the target by the beam causes a drop of a few percent in the polarization, and the polarization slowly decreases with time due to radiation damage. Most of the radiation damage can be repaired by periodically annealing the target, until the accumulated dose reached is greater than about 0.5×10^{17} e^-/cm^2, at which time the target material needs to be replaced.

2.3.1. Polarization Analysis

The three Zeeman sublevels of the deuteron system ($m = -1, 0, 1$) are shifted unevenly due to the quadrupole interaction [23]. This shift depends on the angle between the magnetic field and the electrical field gradient, and gives rise to two separate transition energies. Hence, the unique

double peaked response displayed in Fig. 6. When the system is at thermal equilibrium with the solid lattice, the deuteron polarization is known from:

$$P_z = \frac{4 + \tanh \frac{\mu B}{2kT}}{3 + \tanh^2 \frac{\mu B}{2kT}} \tag{12}$$

where μ is the magnetic moment, and k is Boltzmann's constant. The vector polarization can be determined by comparing the enhanced signal with that of the TE signal (which has known polarization). This polarimetry method is typically reliable to about 3.9% relative.

Similarly, the tensor polarization is given by:

$$P_{zz} = \frac{4 + \tanh^2 \frac{\mu B}{2kT}}{3 + \tanh^2 \frac{\mu B}{2kT}} \tag{13}$$

From Eqs. 12 and 13, we find:

$$P_{zz} = 2 - \sqrt{4 - 3P_z^2} \tag{14}$$

In addition to the TE method, polarizations can be determined by analyzing NMR lineshapes as described in [24] with a typical 7% relative uncertainty. At high polarizations, the intensities of the two transitions differ, and the NMR signal shows an asymmetry R in the value of the two peaks, as shown in Fig. 6. The vector polarization is then given by:

$$P_z = \frac{R^2 - 1}{R^2 + R + 1} \tag{15}$$

and the tensor polarization is given by:

$$P_{zz} = \frac{R^2 - 2R + 1}{R^2 + R + 1} \tag{16}$$

This measuring technique can be used as a compliment to the TE method resulting in reduced uncertainty in polarization.

2.3.2. Tensor Polarization Enhancement

We've assumed a tensor polarization of 25% in this proposal. This is just the tensor polarization that occurs in a standard P_z= 56% vector polarized ND_3 target according to Eq. 14. This enables a

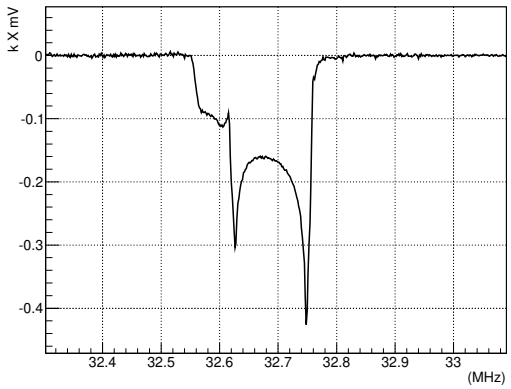

FIG. 7. The deuterium magnetic resonance line shape showing the achievement of high tensor polarization of deuterated butanol after RF saturation of a pedestal at the UVA polarized target lab accomplished during their April 2014 cool-down.

significant measurement of A_{zz}, as shown in Fig. 4. Any improvement to the expected polarization, although not strictly necessary, would allow the addition of kinematic points, and/or improved statistical accuracy.

With this in mind, we note that there is a concerted effort at the University of New Hampshire and the University of Virginia to directly enhance tensor polarization by disturbing the thermal equilibrium of the sample using a frequency modulated RF source to stimulate transitions from the m=0 level. This technique is known as semi-selective RF saturation. This changes the population of the m=0 level, thus changing the tensor asymmetry. This method of 'hole burning' the NMR line with a saturating RF field was demonstrated by deBoer [26], and Meyer [23, 27] in 1985, with more recent successes demonstrated at both UNH and UVa.

2.4. Overhead

Table V summarizes the expected overhead, which sums to 4.9 days. The dominant overhead comes from switching from the polarized to unpolarized state and vice versa, and target anneals.

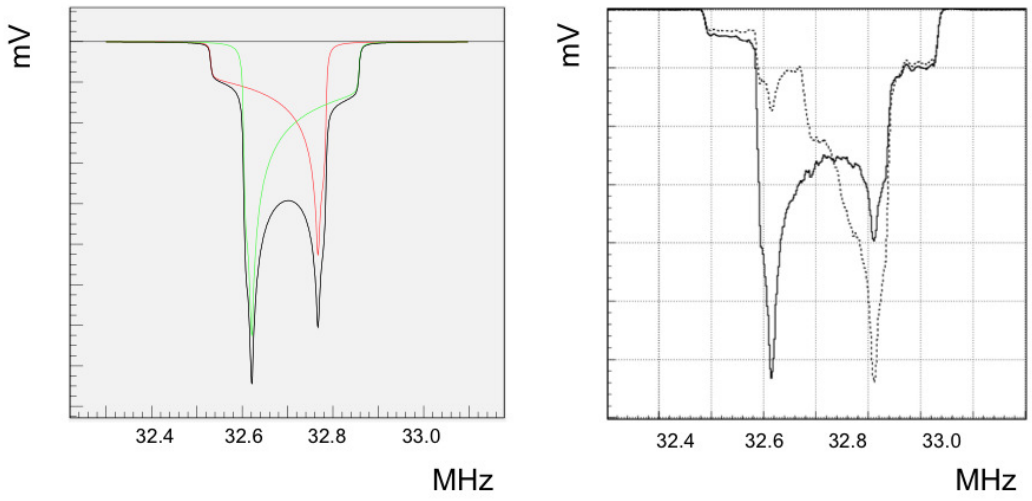

FIG. 8. **Left**: Model prediction [24] of the NMR response for an ND_3 sample. The two discrete transitions (red and green) blend into the characteristic double peaked structure. **Right** : Demonstration of RF hole burning in ND_3. Solid line: ND_3 sample with about 30% vector polarization. Dashed line: the same sample after application of a saturating RF field, which raised the tensor polarization to $P_{zz} \approx 30\%$. Notice the strong suppression of the left peak. Reproduced from [25].

The target will need to be annealed about every other day, and the material replaced once a week. Measurements of the dilution from the unpolarized materials contained in the target, and of the packing fraction due to the granular composition of the target material will be performed with a carbon target.

3. Summary

We have investigated the possibility of making high precision measurements of the quasi-elastic tensor asymmetry A_{zz} using the SoLID detector. By covering the kinematic range from the QE peak ($x = 1$) up to elastic scattering ($x = 2$), we expect that this data will provide valuable new insights about the high momentum components of the deuteron wavefunction. Additionally, we

Overhead	Number	Time Per (hr)	(hr)
Polarization/depolarization	18	2.0	36.0
Target anneal	7	4.0	28.0
Target T.E. measurement	3	4.0	12.0
Target material change	2	4.0	8.0
Packing Fraction/Dilution runs	9	1.0	9.0
BCM calibration	4	2.0	8.0
Optics	2	4.0	8.0
Linac change	1	8.0	8.0
			4.9 days

TABLE V. Major contributions to the overhead.

will obtain A_{zz} data down through the resonance and DIS region to better exerimentally cover the entire kinematic region.

We have found that with 14 days of beam and an additional 4.9 days of overhead, A_{zz} can be measured with high precision at $0.1 < x \leq 2$ in Hall A using SoLID. This experiment can run simultaneously with the co-proposed b_1 measurement.

[1] L. Frankfurt and M. Strikman, Phys.Rept. **160**, 235 (1988).

[2] M. Sargsian, private communication, to be published.

[3] J. L. Forest et al., Phys. Rev. **C54**, 646 (1996), nucl-th/9603035.

[4] J. Arrington, D. Higinbotham, G. Rosner, and M. Sargsian, Prog.Part.Nucl.Phys. **67**, 898 (2012), 1104.1196.

[5] L. L. Frankfurt and M. I. Strikman, Phys. Rept. **76**, 215 (1981).

[6] L. Frankfurt, M. Strikman, D. Day, and M. Sargsian, Phys.Rev. **C48**, 2451 (1993).

[7] J. Arrington, C. Armstrong, T. Averett, O. K. Baker, L. de Bever, et al., Phys.Rev.Lett. **82**, 2056 (1999), nucl-ex/9811008.

[8] N. Fomin, J. Arrington, R. Asaturyan, F. Benmokhtar, W. Boeglin, et al., Phys.Rev.Lett. **108**, 092502 (2012), 1107.3583.

[9] M. Garcon and J. Van Orden, Adv.Nucl.Phys. **26**, 293 (2001), nucl-th/0102049.

[10] S. Veerasamy and W. N. Polyzou, Phys. Rev. C **84**, 034003 (2011), URL `http://link.aps.org/doi/10.1103/PhysRevC.84.034003`.

[11] F. Gross, Phys.Rev. **C26**, 2203 (1982).

[12] W. Buck and F. Gross, Phys.Rev. **D20**, 2361 (1979).

[13] L. Frankfurt and M. Strikman, Nucl.Phys. **B148**, 107 (1979).

[14] L. Alexa et al. (Jefferson Lab Hall A Collaboration), Phys.Rev.Lett. **82**, 1374 (1999), nucl-ex/9812002.

[15] J. Van Orden, N. Devine, and F. Gross, Phys.Rev.Lett. **75**, 4369 (1995).

[16] M. M. Sargsian, Phys.Rev. **C82**, 014612 (2010), 0910.2016.

[17] F. Gross and A. Stadler, Phys.Rev. **C82**, 034004 (2010), 1007.0778.

[18] P. Bosted and V. Mamyan, e-print **arXiv:1203.2262** (2012), 1203.2262.

[19] M. Sargsian, private communication.

[20] D. Keller, Nucl. Inst. and Meth. **A728**, 133 (2013).

[21] D. Keller, XVth International Workshop on Polarized Sources, Targets, and Polarimetry **PoS(PSTP2013)010** (2013).

[22] C. Keith, JLab polarized target group. Private communication.

[23] W. Meyer et al., Nucl. Instrum. Meth. **A244**, 574 (1986).

[24] C. Dulya et al. (Spin Muon), Nucl. Instrum. Meth. **A398**, 109 (1997).

[25] S. Bueltmann, D. Crabb, Y. Prok. *UVa Target Studies*, UVa Target Lab technical note, 1999.

[26] W. de Boer, Cern Report CERN-74-11 (1974).

[27] W. Meyer and E. Schilling, BONN-HE-85-06, C84-09-03.1 (1985).